Holotomography versus X-ray grating interferometry: A comparative study

I. Zanette, S. Lang, A. Rack, M. Dominietto, M. Langer et al.

Citation: Appl. Phys. Lett. **103**, 244105 (2013); doi: 10.1063/1.4848595
View online: http://dx.doi.org/10.1063/1.4848595
View Table of Contents: http://apl.aip.org/resource/1/APPLAB/v103/i24
Published by the AIP Publishing LLC.

Holotomography versus X-ray grating interferometry: A comparative study

I. Zanette,[1,2,a)] S. Lang,[3] A. Rack,[2] M. Dominietto,[4] M. Langer,[5] F. Pfeiffer,[1] T. Weitkamp,[6] and B. Müller[3]

[1]*Physics Department, Technische Universität München, Garching, Germany*
[2]*European Synchrotron Radiation Facility, Grenoble, France*
[3]*Biomaterials Science Center, University of Basel, Basel, Switzerland*
[4]*Institute for Biomedical Engineering, ETH Zürich, Zürich, Switzerland*
[5]*Université de Lyon, Creatis, CNRS UMR 5220, INSERM U 1022, Université Lyon 1, INSA Lyon, Villeurbanne, France*
[6]*Synchrotron Soleil, Gif-sur-Yvette, France*

(Received 5 September 2013; accepted 29 November 2013; published online 11 December 2013)

X-ray phase-contrast imaging techniques are used at synchrotron facilities to visualize tiny density variations in bulk samples. They overcome the limitations of other non-destructive methods, which often provide insufficient spatial and/or density resolution. Holotomography (HT) and X-ray grating interferometry (XGI) are among the most powerful phase-contrast techniques. Here, we show a direct comparison of HT versus XGI. We find that XGI excels in fidelity of the density measurements and is more robust against low-frequency artifacts, while HT is superior in spatial resolution. This study gives indications for applications and developments of phase-contrast imaging. © *2013 AIP Publishing LLC*. [http://dx.doi.org/10.1063/1.4848595]

Phase-contrast X-ray imaging techniques are used, especially at synchrotron radiation facilities, to visualize and quantify tiny density variations in bulk objects, with applications in materials science, biomedical engineering, and beyond. To generate the image signal, phase-contrast imaging relies on the phase shift that X-rays undergo while passing through matter. As the phase-shift cross section of all materials for hard X rays is much larger than their absorption cross section, phase-contrast imaging techniques overcome the limitations of conventional absorption imaging, which often provide insufficient density resolution.[1]

Various phase-contrast imaging techniques have been developed in the last decades.[2–4] They differ in the mechanism used to detect the phase shift, in the physical quantity recorded in the raw data, in the spatial resolution (SR) accessible in the final images, and in the X-ray beam and detector requirements. Three-dimensional imaging based on holotomography[5] (HT) and X-ray grating interferometry[6,7] (XGI) yields the refractive index decrement δ, proportional to the electron density,[8] throughout the specimen. HT and XGI perform well over a large energy range and do not require a strictly monochromatic or parallel beam. They can provide ultra-high density resolution at microscopic length scales and over a field of view of a few centimeters.[9,10] Because of their performance in non-destructive three-dimensional imaging, HT and XGI are used for a wide range of applications at many synchrotron beamlines.

In this paper, we discuss the advantages and limitations of HT and XGI relative to each other and quantitatively compare tomograms of soft-tissue biological specimens with respect to density resolution and spatial resolution. Considerations in the presence of image artifacts and on the correctness of the δ measurements are also presented.

Holotomography is a free-space propagation method, i.e., it does not require any optical element between sample and detector (Fig. 1(a)).[5] The phase is retrieved from a series of n_{HT} holograms taken at a few predefined sample-to-detector distances d_h. Although these distances are chosen so that different spatial frequencies are mapped with similar intensity in the retrieved phase data,[11] problems remain with low-spatial frequencies which are poorly transferred in the Fresnel-diffraction images.[12] Among the different algorithms that have been developed to retrieve the phase from the HT data, we have used the one proposed by Guigay *et al.*,[13] based on a combination of the contrast-transfer-function approach and the transport-of-intensity equation. To increase the information in the low-spatial frequency range, we have used a refinement of this algorithm to make it more robust in the low-spatial frequency range:[14] an *a priori* estimation of the ratio δ/β (with β being the imaginary part of the X-ray refractive index) is used for those frequencies for which phase contrast is insufficient. This stabilizes the reconstruction yet does not impose the condition of constant δ/β on all length scales. This algorithm has proved to yield reliable and robust results.[15]

Unlike HT, XGI uses special X-ray optical components. An X-ray grating interferometer consists of two line gratings placed between sample and detector (Fig. 1(b)). The first of these gratings, G1, typically a phase grating (here made of silicon), induces a modulation in the phase profile of the wavefront.[18] The second grating, G2, has absorbing gold lines and acts as an analyzing transmission mask.[6] The period p_1 of G1 is chosen so that the interference pattern produced by this grating at the position of G2, placed at a distance d_g from G1, matches the period p_2 of G2. In the presence of an object, the interference lines from G1 are distorted and contain information on the optical properties of the sample. Among this information, the differential phase contrast (DPC) signal is related to the lateral displacement of the interference fringes. It can be extracted and separated from other contributions with the phase-stepping technique, in which a series of n_{XGI} images is collected at different

a)irene.zanette@tum.de

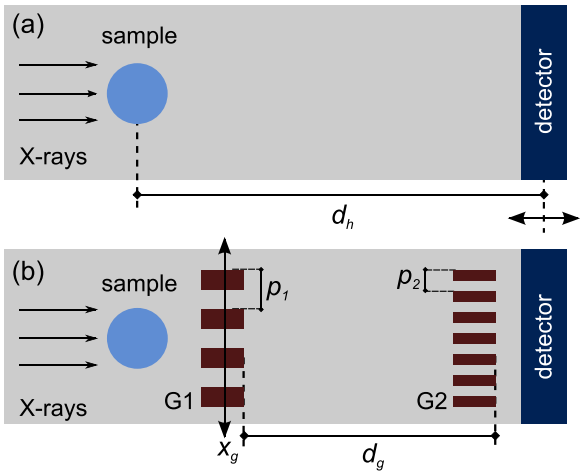

FIG. 1. Schematic representation of a holotomography setup (a) and an X-grating interferometry setup (b).

lateral positions of one of the two gratings. These images are usually processed with a pixel-wise Fourier analysis.[7,19]

The tomography measurements were performed at the beamline ID19 of the European Synchrotron Radiation Facility (ESRF), Grenoble, France, with the parameters reported in Table I. In these measurements, the image detector was a CCD camera coupled to a converter screen with a lens system. The quantity h_{HT}/h_{XGI} in Table I is the ratio of the number of photons per voxel used in the two scans: $h_{HT}/h_{XGI} = (t_{HT} \times N_{HT} \times n_{HT} \times \Delta_{HT}^2)/(t_{XGI} \times N_{XGI} \times n_{XGI} \times \Delta_{XGI}^2)$, where Δ indicates the pixel size.

The biological samples used for this study were a tumor of human cells grown in a nude mouse and a heart of a rat without any pathological symptom. Both specimens were immersed in formalin solution for preservation and placed in plastic cylindrical containers that were fixed on the sample stage.[20] The container of the heart was immersed in a water bath to avoid phase-wrapping artifacts in XGI. For the tumor measurement, these artifacts were corrected algorithmically prior to tomographic reconstruction.[21]

Phase and DPC projections from the HT and XGI scans were retrieved as described above. To retrieve the holotomographic phase projections, δ/β was set to 1372 and to 1546, respectively, for the tumor and heart sample. For both scans, a filtered-backprojection algorithm was used to obtain the tomographic reconstructions of δ.[22,23,33]

Figures 2 and 3 show characteristic HT and XGI tomography slices of, respectively, the tumor and the heart.

The immersion liquid can be clearly distinguished from the tissues, which is difficult with conventional absorption X-ray imaging.[24,25] Moreover, the anatomical features of the tissues are recognized in the HT and XGI data. The HT reconstruction, however, contains prominent low-frequency artifacts. These effects were explained as a result of poor transmission of low spatial frequencies in the Fresnel-diffraction images.[26] Because XGI measures the first and not the second derivative of the phase, this type of artifacts is avoided in the XGI reconstructions. In Fig. 3(a), one also finds remaining edge-enhancement fringes at the interfaces between the sample and the formalin solution.[27]

The quantitative comparison of the contrast of the two methods is based on the evaluation of the contrast-to-noise ratio (CNR) for selected pairs of materials, see Figs. 2 and 3. The CNR can be defined as $|S_a - S_b|/\sqrt{\sigma_a^2 + \sigma_b^2}$, where S indicates the average of a homogeneous region of interest (ROI), and σ indicates its standard deviation.[28] The selected pairs of materials are denoted with the subscripts a and b, where b is the immersion liquid. The results reported in

TABLE I. Experimental parameters. t is the exposure time per frame and N is the number of projections.

	Tumor sample	Heart sample
Insertion device	Undulator	Wiggler
Monochromator	Multilayer	Double crystal
X-ray energy (keV)	17.6	19.0
Pixel size (μm)	3.0	7.5 [HT], 8.0 [XGI]
HT parameters	$n_{HT} = 3$	$n_{HT} = 4$
d_h (m)	0.06, 0.12, 0.36	0.2, 0.4, 0.7, 1.1
XGI parameters	$n_{XGI} = 4$	$n_{XGI} = 5$
$p_1 = 2p_2$ (μm)	4.0	4.8
d_g (mm)	140	482
t (s)	0.3	1.0 [HT], 1.5 [XGI]
N	359 [XGI], 800 [HT]	1499
h_{HT}/h_{XGI}	1.7	0.6

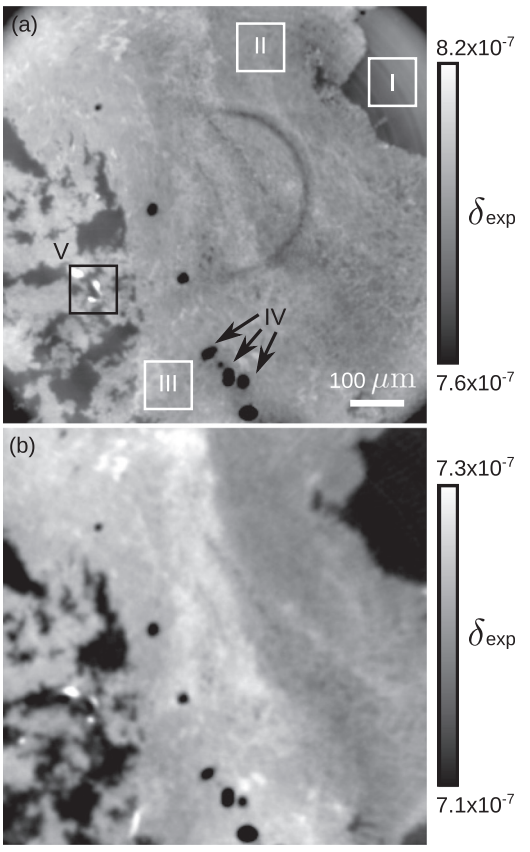

FIG. 2. Region of interest from HT slice (a) of a tumor tissue. The related part of the XGI slice (b) was found by non-rigid 3D registration.[16,17] Anatomical features provided the basis for the CNR and SR measurements: ROI I corresponds to formalin and is used as reference. The variation in the grey levels of the formalin in panel (a) is due to low-frequency artifacts. ROI II to IV contain prominent features. The pin sharp feature V yielded the spatial resolution.

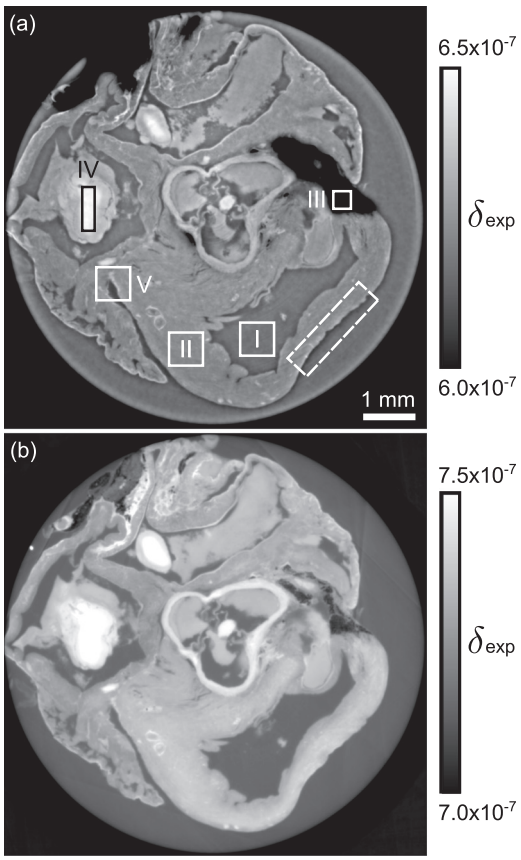

FIG. 3. Phase tomography slices of the rat heart obtained with HT (a) and XGI (b). The tricuspid valve is at the center of the images. The gray scaling has been adjusted to optimize the visualization of the tissue forming the heart. Rectangles II to IV indicate ROIs used for the calculation of the CNR values. ROI V was used to determine the spatial resolution, and ROI I was used as reference for both SR and CNR. The dashed rectangle in panel (a) highlights a region with remaining edge-enhancement fringes.

Table II show that the CNR provided by XGI is overall higher than the one in the HT slices. This is true also for the heart sample, which has been measured with 70% more photons per voxel in HT than in XGI, see Table I.

To understand the difference in the absolute δ values obtained with HT and XGI, the polypropylene container, which enclosed the heart and has a well-defined composition and density, was considered. In the XGI slice, one finds a δ value of $6.06(2) \times 10^{-7}$, which is close to the prediction of 5.90×10^{-7}. The HT measurements show a much lower value of $3.01(4) \times 10^{-7}$, an observation consistent with previous reports on similar cases.[26]

The visual inspection of the HT and XGI data for both specimens reveals that the microstructures appear much sharper in HT, a phenomenon to be quantified. The SR is evaluated using the radial spectral power (RSP). Here, the SR corresponds to the highest spatial frequency for which the RSP of a structure-rich ROI is larger than twice the baseline of a featureless region.[29] The data listed in Table II confirm that HT provides images with better SR than XGI. The limiting factor in XGI is the separation s of the beams diffracted by G1, $s = 2d_g\lambda/p_1$. In our experiments, $s = 9.9\,\mu$m for the tumor scan, and $s = 26.2\,\mu$m for the heart measurement. These values are approximately three times smaller than the SR determined with the RSP method. The SR in HT is also limited by diffraction, and, in particular, by the blurring introduced by the presence of the Fresnel fringes in the projection data.

TABLE II. Values of CNR and SR.

	CNR			SR (μm)
Tumor	Tissue I	Tissue II	Lipid	
HT	14.1	12.4	40.4	10.6
XGI	59.4	54.4	167.8	24.5
Heart	Tissue	Lipid	Blood	
HT	15.9	84.1	114.6	70.0
XGI	54.7	103.8	262.8	81.7

In conclusion, this study presents a quantitative comparison of synchrotron X-ray phase microtomography data obtained with two methods, X-ray grating interferometry and holotomography, and it demonstrates the complementarity of these two techniques. While XGI images have the highest density resolution and show the best accuracy of retrieved values of the refractive index for the known materials, HT provides images with higher spatial resolution. These findings remain true even if the dose is varied. For a spatial resolution better than $10\,\mu$m, HT is the better choice, unless gratings with much smaller periods become widely available.[30] To detect the fringes in propagation-based phase-contrast imaging with large pixels, very long and often impractical propagation distances are required. In these cases, XGI is technically the method of choice.

The two methods are complementary also under the operational point of view. HT has a simpler mechanical implementation, but requires experts for manual data processing. An additional difficulty is that the HT phase retrieval generally relies on the registration of the images taken at different distances. The processing of XGI is fully automatic and it only requires the input of basic experimental parameters such as λ and d_g. The retrieved δ values in XGI are also fully model-independent, which is not the case for the HT reconstruction method used here which requires an estimate of the refractive index of the object. These advantages of XGI come at the expenses of a more complicated set-up and somehow longer data acquisition times. However, acquisition time and dose delivered to the sample can be reduced, while preserving the image quality, with less absorbing grating substrates and/or recent advanced acquisition schemes.[34] In addition, more sophisticated algorithms for HT can substantially reduce some of the artifacts observed in the present study.[26]

It should be mentioned that even simpler propagation-based methods than the multi-distance HT might be used to obtain quantitative phase images. Even data taken at a single distance can be used for this purpose, but these methods are even more dependent on *a priori* knowledge than HT.[31,32] While not the subject of the present paper, these methods can clearly be an alternative to HT and XGI for certain studies.

We acknowledge J. Mohr (KNMF) and J. Kenntner (KNMF), S. Rutishauser (PSI) and C. David (PSI) for providing the gratings, and G. Le Duc (ESRF) for providing the heart specimen. The project was supported by the Swiss National Science Foundation (Grant No. 200021_127297 1).

T.W. acknowledges support from the French research networks (RTRA) "Digiteo" and "Triangle de la Physique" (Grant Nos. 2009-79D and 2009-034T). F.P. acknowledges financial support through the DFG Cluster of Excellence Munich-Centre for Advanced Photonics (MAP), the DFG Gottfried Wilhelm Leibniz program, and the European Research Council (ERC, FP7, StG 240142). This work was carried out with the support of the Karlsruhe Nano Micro Facility (KNMF, www.kit.edu/knmf), a Helmholtz Research Infrastructure at Karlsruhe Institute of Technology (KIT).

[1]R. Fitzgerald, Phys. Today **53**(7), 23 (2000).
[2]U. Bonse and M. Hart, Appl. Phys. Lett. **6**, 155 (1965).
[3]E. Förster, K. Goetz, and P. Zaumseil, Krist. Tech. **15**, 937 (1980).
[4]A. Snigirev, I. Snigireva, V. Kohn, S. Kuznetsov, and I. Schelokov, Rev. Sci. Instrum. **66**, 5486 (1995).
[5]P. Cloetens, W. Ludwig, J. Baruchel, D. V. Dyck, J. V. Landuyt, J. P. Guigay, and M. Schlenker, Appl. Phys. Lett. **75**, 2912 (1999).
[6]A. Momose, S. Kawamoto, I. Koyama, Y. Hamaishi, K. Takai, and Y. Suzuki, Jpn. J. Appl. Phys., Part 2 **42**, L866 (2003).
[7]T. Weitkamp, A. Diaz, C. David, F. Pfeiffer, M. Stampanoni, P. Cloetens, and E. Ziegler, Opt. Express **13**, 6296 (2005).
[8]A. Guinier, *X-ray Diffraction in Crystals, Imperfect Crystals, and Amorphous Bodies*, Dover Books on Physics Series (Dover, 1994).
[9]G. Schulz, T. Weitkamp, I. Zanette, F. Pfeiffer, F. Beckmann, C. David, S. Rutishauser, R. Reznikova, and B. Müller, J. R. Soc. Interface **7**, 1665 (2010).
[10]G. Schulz, C. Waschkies, F. Pfeiffer, I. Zanette, T. Weitkamp, C. David, and B. Müller, Sci. Rep. **2**, 826 (2012).
[11]S. Zabler, P. Cloetens, J.-P. Guigay, J. Baruchel, and M. Schlenker, Rev. Sci. Instrum. **76**, 073705 (2005).
[12]H. Bremmer, Physica **18**, 469 (1952).
[13]J. P. Guigay, M. Langer, R. Boistel, and P. Cloetens, Opt. Lett. **32**, 1617 (2007).
[14]M. Langer, P. Cloetens, and F. Peyrin, IEEE Trans. Image Process. **19**, 2428 (2010).
[15]M. Langer, P. Cloetens, J. Guigay, and F. Peyrin, Med. Phys. **35**, 4556–4566 (2008).
[16]A. Andronache, M. von Siebenthal, G. Szekely, and P. Cattin, Med. Image Anal. **12**, 3 (2008).
[17]B. Müller, H. Deyhle, S. Lang, G. Schulz, T. Bormann, F. Fierz, and S. Hieber, Int. J. Mater. Res. **103**, 242 (2012).
[18]C. David, B. Nöhammer, H. H. Solak, and E. Ziegler, Appl. Phys. Lett. **81**, 3287 (2002).
[19]A. Momose, Jpn. J. Appl. Phys., Part 1 **44**, 6355 (2005).
[20]The heart specimen was extracted from a Fischer rat at ESRF with procedures conformed to the guidelines of the French Government. After extraction, the heart was immersed in a 10% formalin solution and placed in a plastic container. The tumor was injected on the flank of a Balb nude mouse and was extracted from the animal before it had reached a diameter of 3 mm. All procedures regarding the tumor growing and extraction were performed in strict adherence to the Swiss law for animal protection. The tumor was fixed in formalin 5% solution and placed in a plastic capillary.
[21]I. Zanette, T. Weitkamp, S. Lang, M. Langer, J. Mohr, C. David, and J. Baruchel, Phys. Status Solidi A **208**, 2526–2532 (2011).
[22]The quantitative δ values were obtained by adding an offset corresponding to the theoretical δ values of the immersion material at the working energies (δ of water at 19 keV is 6.39×10^{-7} and δ of air at 17.6 keV is 7×10^{-10} from the Henke database[33]).
[23]F. Pfeiffer, C. Kottler, O. Bunk, and C. David, Phys. Rev. Lett. **98**, 108105 (2007).
[24]P. Cloetens, R. Mache, M. Schlenker, and S. Lerbs-Mache, Proc. Natl. Acad. Sci. U.S.A. **103**, 14626 (2006).
[25]T. Weitkamp, C. David, O. Bunk, J. Bruder, P. Cloetens, and F. Pfeiffer, Eur. J. Radiol. **68**, S13 (2008).
[26]M. Langer, P. Cloetens, A. Pacureanu, and F. Peyrin, Opt. Lett. **37**, 2151 (2012).
[27]Data taken at propagation distances shorter than 20 cm could not be used for the reconstruction because the absorption signal was too weak for the alignment with the other data. Using the pure absorption image would have helped to reduce the edge-enhancement artifacts.
[28]J. Herzen, T. Donath, F. Pfeiffer, O. Bunk, C. Padeste, F. Beckmann, A. Schreyer, and C. David, Opt. Express **17**, 10010 (2009).
[29]P. Modregger, D. Lübbert, P. Schäfer, and R. Köhler, Phys. Status Solidi A **204**, 2746 (2007).
[30]H. Wen, D. E. Wolfe, A. A. Gomella, H. Miao, X. Xiao, C. Liu, S. K. Lynch, and N. Morgan, Rev. Sci. Instrum. **84**, 013706 (2013).
[31]D. Paganin, S. C. Mayo, T. E. Gureyev, P. R. Miller, and S. W. Wilkins, J. Microsc. **206**, 33 (2002).
[32]M. Beltran, D. Paganin, K. Uesugi, and M. Kitchen, Opt. Express **18**, 6423 (2010).
[33]B. Henke, E. Gullikson, and J. Davis, At. Data Nucl. Data Tables **54**, 181 (1993).
[34]I. Zanette, M. Bech, A. Rack, G. Le Duc, P. Tafforeau, C. David, J. Mohr, F. Pfeiffer, and T. Weitkamp, Proc. Natl. Acad. Sci. **109**, 10199–10204 (2012).